AFRL-AFOSR-JP-TR-2022-0012

Lightweight, Energy Ansorbing Sandwich Composite Structures with Bamboo Fiber Reinforced Plastic (BFRP) Core by using Additive Manufacturing

Suhr, Jonghwan
Sungkyunkwan University Research & Business
2066 Seobu-ro, Jangan-gu
Suwon,, , 16419
KR

01/09/2022
Final Technical Report

Air Force Research Laboratory
Air Force Office of Scientific Research
Asian Office of Aerospace Research and Development
Unit 45002, APO AP 96338-5002

REPORT DOCUMENTATION PAGE

PLEASE DO NOT RETURN YOUR FORM TO THE ABOVE ORGANIZATION.

1. REPORT DATE	2. REPORT TYPE	3. DATES COVERED	
20220109	Final	START DATE 20190619	END DATE 20210618

4. TITLE AND SUBTITLE
Lightweight, Energy Ansorbing Sandwich Composite Structures with Bamboo Fiber Reinforced Plastic (BFRP) Core by using Additive Manufacturing

5a. CONTRACT NUMBER	5b. GRANT NUMBER	5c. PROGRAM ELEMENT NUMBER
FA2386-19-1-4029		61102F
5d. PROJECT NUMBER	**5e. TASK NUMBER**	**5f. WORK UNIT NUMBER**

6. AUTHOR(S)
Jonghwan Suhr

7. PERFORMING ORGANIZATION NAME(S) AND ADDRESS(ES)
Sungkyunkwan University Research & Business
2066 Seobu-ro, Jangan-gu
Suwon, 16419
KR

8. PERFORMING ORGANIZATION REPORT NUMBER

9. SPONSORING/MONITORING AGENCY NAME(S) AND ADDRESS(ES)	10. SPONSOR/MONITOR'S ACRONYM(S)	11. SPONSOR/MONITOR'S REPORT NUMBER(S)
AOARD UNIT 45002 APO AP 96338-5002	AFRL/AFOSR IOA	AFRL-AFOSR-JP-TR-2022-0012

12. DISTRIBUTION/AVAILABILITY STATEMENT
A Distribution Unlimited: PB Public Release

13. SUPPLEMENTARY NOTES

14. ABSTRACT
Sandwich structures are extensively employed in lightweight parts/structures of military aircraft because of their high specific strength and stiffness. One undesirable property of sandwich structures is that they perform poorly with respect to energy absorption, and that can cause negative effects on vibrational damping, noise, and impact resistance. In this project, bamboo fiber reinforced plastic (BFRP) and additive manufacturing, also known as 3D printing, were suggested as a new core material and manufacturing technology in order to improve the energy absorption properties of sandwich structures. Bamboo fiber with its intriguing properties and sustainability has received significant interest as a reinforcement of fiber composites. Here, the bamboo fiber extraction technique along with a thorough understanding of the bamboo fiber as a reinforcement of polymer composite has been investigated to develop BFRP composites which have high strength and energy absorption.

15. SUBJECT TERMS

16. SECURITY CLASSIFICATION OF:			17. LIMITATION OF ABSTRACT	18. NUMBER OF PAGES
a. REPORT U	b. ABSTRACT U	c. THIS PAGE U	SAR	32

19a. NAME OF RESPONSIBLE PERSON	19b. PHONE NUMBER *(Include area code)*
TONY KIM	315-227-7008

TABLE OF CONTENTS

Section Page

LIST OF FIGURES

Page

LIST OF TABLES

Page

1.0 SUMMARY

This project investigated the bamboo fiber reinforced plastic (BFRP) as a material for additive manufacturing, also known as 3D printing. Bamboo fiber has received significant interest as a reinforcement of fiber composites due to its intriguing properties and sustainability. Here, we explore bamboo fibers as reinforcement in polymer composites to develop BFRP composites with enhanced mechanical properties. Although the project has the scope of 2 years when the proposal submitted, we performed only 1 year due to the funding condition.

Year 1: Synthesis of Bamboo Fiber Reinforced Polymer Composites

(1) Bamboo fiber surface modification and its composites: Mercerization, Acetylation, and Plasma treatment

(2) Extraction of cellulose nanofibrils(CNFs) from bamboo, and NR/CNFs bio-composites

Among the pretreatments to increase the interfacial strength of the matrix and bamboo fibers in composites, acetylation was the most effective, and the modulus value increased by 53.6% compared to pure PLA.

For CNFs, those were successfully isolated from bamboo using microwave liquefaction combined with HPAC delignification, alkaline treatment, acid hydrolysis, and low energy nanofibrillation. The obtained CNFs contain 94.52% cellulose and 0.61% hemicellulose with no lignin detected and a yield of 22.52%. NR/CNF nanocomposites were formed by adding CNFs into the rubber matrix, using latex mixing, compound mastication, and vulcanization. The tensile strength, toughness, and cross-link density values were the highest for the NR/CNF10 sample. The DMA analysis indicated that the addition of CNFs increased the storage modulus of the nanocomposites at the glassy state and the rubbery state. Consequently, the presented results concluded that the obtained CNFs seem to be potential green reinforcements for NR-based nanocomposites without any surface modification needed.

Although bamboo fibers have outstanding characteristics, significant challenges still remain in developing 3D printable BFRP composites for manufacturing core structures. Note that this task was planned for the second year.

2.0 INTRODUCTION

Sandwich structures are substantially employed in military aircraft structures, including wings, cabin doors, cabin walls, flooring, fairings, and others. Such sandwich structures are composite systems made by adhesively bonding two relatively thin, strong, and stiff face sheets between a relatively weaker and thick lightweight core structure. The face sheets mainly resist bending stress while the core structure experiences shear stress. Although it presents promising performances, they exhibit very poor vibrational damping, noise, and impact resistance. Such unfavorably poor energy absorbing properties can often lead to serious detrimental effects, including radiation of unwanted noise, the proliferation of vibrations that can shorten the lifespan of the composites, and high susceptibility to damage due to impact. Therefore, in order to improve energy absorbing properties of sandwich composite structures, a number of core materials and geometries have been suggested, including honeycomb and synthetic foams as core materials.

Traditionally, carbon fiber reinforced plastic (CFRP) is mainly used as a core material for

sandwich composites. Carbon fibers (CFs) are used as a reinforcement of a polymer filament for the fused deposition modeling (FDM) 3D printing technique with its extraordinary mechanical properties. However, the production of CFs relies on non-renewable petroleum feedstock and also has high energy costs. Moreover, the high rate of depletion of petroleum resources has forced the development of new reinforced materials for polymer composites that are green, sustainable, and compatible with the environment [1, 2]. Among the various natural fibers, short bamboo fibers were selected as reinforcement materials in the polymer matrix for the following reasons. First, bamboo has the fastest growth rate among the various types of renewable natural fibers. Second, the cellulose fibers in bamboo are aligned along the length of the bamboo providing maximum tensile strength, flexural strength, and rigidity in that direction. However, cellulose is strongly bonded in the matrix of lignin and hemicellulose in bamboo, so removing non-cellulosic components is troublesome [3−7]. Several chemical pretreatments like bleaching, alkaline pretreatment, acid hydrolysis, steam explosion, enzymatic pretreatment, ionic liquids, TEMPO (2,2,6,6-tetramethyl piperidin-1-oxidany) oxidation have been applied to remove non-cellulosic components from the bamboo [8−11].

The surface condition and chemical composition of the natural fiber can be manipulated by chemical treatment to obtain the desired property [12]. Among the chemical often used for natural fiber treatment are sodium hydroxide (NaOH) [13, 14], nitric acid and potassium chlorate (HNO_3–$KClO_3$) [15], sodium hypochlorite (NaClO) [16], and benzoate[17]. Alkali treatment is known as the most commonly used and relatively inexpensive chemical treatment [18-20]. Meanwhile, reinforced composites obtained with acetylated BF show better mechanical properties due to the grafting of acetyl groups onto the cellulose fiber surface and thus improve compatibility between BF and matrix [21]. The main defect of BF is the lack of adhesion to hydrophobic polymers. The hydrophilic nature of fiber surfaces results in a low interaction with hydrophobic polymers. Physical and chemical fiber surface treatments improve adhesion between the polymer and the surface of the fibers by reducing the polarity or changing the polarity of the fiber surface [22-25]. For this reason, the use of plasma was also considered a more environmentally friendly approach. The plasma state opens up new possibilities for efficiently functionalizing even the most inert polymeric substrates. In recent years, there has been increasing interest in the use of plasmas for in situ polymer synthesis and surface modification of films and fibers [26].

In this study, bamboo fiber reinforced plastic (BFRP) was explored as a core material, and additive manufacturing was employed in order to create a core structure for the future plan. As mentioned above, the mechanical properties of BFRP treated by various methods of surface modification studied recently were comparatively analyzed to confirm the possibility of its application as additive manufacturing filament material.

3.0 METHODS, ASSUMPTIONS, AND PROCEDURES

3.1 Materials

2~3-year-olds Henon Bamboo was provided by Myeongseok Bamboo, South Korea, which was used as a cellulose source. PLA pellets were purchased from Natural Works, USA. Diethylene glycol (DEG, 99%) and sodium hydroxide (NaOH, ≥98%) were purchased from Sigma-Aldrich, USA. Dioxane ($C_4H_8O_2$, 99.5%), hydrogen peroxide (H_2O_2, 30%), potassium hydroxide (KOH, 93%), glacial acetic acid (AA, 99%), and sulfuric acid (H_2SO_4, 95%), acetic anhydride ($C_4H_6O_3$, ≥99%) were purchased from Daejung Chemical & Metals Co., Ltd., Korea. All chemicals were used as analytical reagent grade without further purification.

3.2 Fiber Extraction

TinyCNC-3035C (TINYROBO Co., Ltd., South Korea) was used to extract the bamboo fiber. The milling tool used in the experiments was a square type with two straight flutes of tungsten steel. The end-mill diameter was 6 mm. Table 1 shows the machining conditions [27]. The tool followed a spiral path from the perimeter to the center with a cutting depth of 0.05 mm per one cycle in the radius direction of the bamboo stem, as shown in Fig. 1.

Table 1. Machining conditions.

Description	Value	Unit
Spindle speed (S)	5,000	rpm
Feed speed (F)	500	mm/min
Depth of cut in radius direction (R_v)	0.05	mm
Depth of cut in bamboo fiber direction (A_d)	5	mm
End-mill radius (r)	3	mm
Number of end-mill cutting edge (Z)	2	ea.

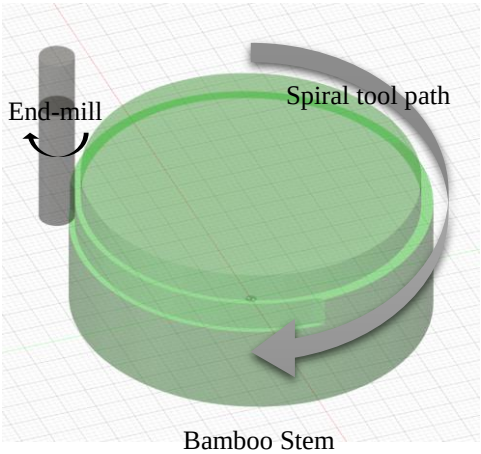

Figure 1. A schematic of a spiral tool path.

3.3 Fiber Surface Modification

3.3.1 Mercerization

Mercerization is one of the alkali treatments that is widely used in cellulose fiber processing using NaOH. The main purpose of alkali pretreatment is to remove the lignin and other impurities. Raw bamboo fibers were mercerized with four different concentrations (i.e., 2, 5, 10, and 15 wt% of NaOH solution) at room temperature for an hour. After washing it in deionized water at room temperature for 15 min, it was neutralized to pH 6.5 to 7 using acetic acid and then dried in an oven at 70°C for overnight to remove the moisture.

3.3.2 Acetylation

The hydrophilic properties of cellulosic materials cause problems when they are used as reinforcement in plastics [28]. The hydrophilicity of cellulose influences their durability and the interfacial adhesion between fiber and polymers. Acetylation used to decrease the

hydrophilicity and increase the weathering resistance of cellulose to this project. The main principle of the acetylation method is to react the hydroxyl groups (OH) of fiber with acetyl groups (CH_3COO^-), thereby rendering the fiber surface more hydrophobic [29]. Non-catalyzed room temperature acetylation method was employed to simplify the process in this study. First, 30 g of bamboo fibers were soaked in a beaker containing 1,800 ml of 15% acetic acid for 50 min. Then, washed fibers were transferred and soaked to a beaker containing 1,500 ml of 5% acetic anhydride for 30 min. Finally, acetylated fibers were washed with running water until acid-free and dried in an oven at 70°C for 24 hours.

3.3.3 Plasma Treatment

The surface property of the fiber relates to physical-mechanical properties indirectly. When applying natural fibers to the composite, there was a problem of compatibility with the polymer resin. Bamboo fibers exhibited hydrophilicity due to hydroxyl groups (-OH) of cellulose, which has been reported the mercerization increases the hydrophilicity. On the other hand, PLA exhibited hydrophobicity. Due to this, the compatibility (interface adhesion properties) between the polymer resin and natural fibers was confirmed as poor adhesion, resulting in degraded physical properties. Hydrophilic and hydrophobic materials are defined by the geometry of water on a flat surface, specifically, the angle between a droplet's edge and the surface underneath it. Moreover, the wettability of a material's surface plays a significant role in interacting with such surfaces. Hydrophobic treatment on the bamboo panel using atmospheric pressure plasma (IHP-1000, APP Co., Ltd., South Korea) was attempted as an eco-friendly approach to fiber surface modification. In order to measure the contact angle of bamboo, polished flat bamboo panel was prepared as shown in Fig. 2. C_4F_8 (Octafluorocyclobutane) was used to impart hydrophobicity to bamboo fiber as a reaction gas, and He (Helium) was used as a carrier gas.

Figure 2. Dimensions of a Bamboo panel.

Table 2. Plasma treatment condition.

	Description	
Gas	Carrier gas	Reaction gas
	He	C_4F_8
Gas flow	14 L/min	4.5 mL/min
Speed	30 mm/s	
Acc/Dec	0.1 sec	
RF-Power	120 W	

3.4 Preparation of Bamboo Fiber Reinforced PLA (BFRP) Composites

The preparation of composites was carried out by dry blending in Haake Rheomix 600 (Thermo Scientific, USA). Mixing conditions were 180°C for 15 min.

3.5 Preparation of Cellulose Nanofibrils

3.5.1 Liquefaction of bamboo under microwave irradiation

The liquefaction reaction of bamboo was performed in a microwave oven (SK Magic, MWO−18M1, 700 W, 2.45 GHz, South Korea). DEG was used as liquefaction solvent with bamboo to solvent ratio of 1/4 (w/w), while H_2SO_4 was used as catalyst (3 wt.% of solvent weight). All reagents (bamboo, DEG, and H_2SO_4) were loaded in a 250 mL Erlenmeyer flask covered with a glass cap. The reaction was conducted at a fixed power of 250 W for 8 min. After the reaction, the mixture was immediately cooled to room temperature, diluted with dioxane/water solution (8/2, v/v), and then vacuum-filtered to separate the solid residues and the liquid mixture. Then, the residues were washed with deionized water and then oven-dried at 90℃ for 24 h.

3.5.2 Chemical treatments of the residues and preparation of cellulose nanofibrils

The microwave-liquefied residues were immersed in hydrogen peroxide-acetic acid (HPAC) solution containing H_2O_2 and AA in a 2/1 (v/v) ratio. The delignification reaction was conducted in an oil bath at 85℃ for 2 h. In the next step, the delignified fibers were treated with 5 % (w/v) KOH solution at 85℃ for 2 h in order to obtain CFs. The fibers were then subjected to acid hydrolysis with 2% (v/v) H_2SO_4 solution at 75℃ for 1 h, followed by centrifugation steps at 3,500 rpm for 20 min to remove the residual acid and collect the sediment. Finally, the sediment was diluted with deionized water and put in the ultrahigh speed blender (Koselig, YB-S03G, Philips, Netherlands) at a constant speed of 24,000 rpm and a power of 1,800 W. The nanofibrillation process was conducted for 30 min. The suspension was then freeze-dried for 48 h to obtain powders. The yield of CNFs was calculated as the mass percentage of the freeze-dry CNFs to the bamboo.

3.6 Preparation of NR/CNFs Bio-composites

NR/CNFs bio-composites were fabricated by two-step techniques, including demulsification process, compound mixing combined with vulcanization. In the first step, the appropriate m-CNFs suspension was added drop-wise into NR latex, followed by a 30 min ultrasonication and another 30 min of magnetic stirring to form a uniform dispersion of m-CNF into NR chains. Subsequently, the mixture was precipitated and coagulated by adding 1 wt.% of H_2SO_4 solution and immersed in deionized water for 24 h to remove the remaining acid. The obtained compound was air-dried at 60℃ overnight. In the next step, a certain amount of stearic acid and ZnO was loaded into the internal mixer along with NR and NR/CNFs bio-composites. The mixing process was conducted at 100℃ with a speed of 60 rpm for 8 min. After that, the vulcanized reagents (sulfur, CBS, and DPG) were added into the internal mixer and well-mixed at 40℃ with a speed of 60 rpm for 10 min. The compounding sheets were then vulcanized at 160℃ in a hot press. The formulations of NR/CNFs bio-composites are shown in Table 3.

Table 3. Formulations of NR/CNFs bio-composites.

Ingredients	**Loading (phr*)**
NR	100
CNFs	Varied (0, 5, 10, 15)
Stearic acid	2
ZnO	3
Sulfur	2.5

CBS	1.5
DPG	2

3.7 Characterization

Mechanical properties were measured by Instron E3000 (Instron Co., Norwood, MA, USA) according to the American Society for Testing and Materials (ASTM) D638-V. Chemical compositions of the samples were determined according to the following ASTM standards: holocellulose (ASTM D1104-56), cellulose (ASTM D 103-60), and lignin (ASTM D1106-56). Hemicellulose was determined by the difference between holocellulose and cellulose content. Fourier-transform infrared (FTIR) spectra were recorded using IFS−66/S, TENSOR27 instrument (Bruker Co., Germany) in the scanning wavenumber region from 400 to 4,000 cm^{-1}, with a resolution of 4 cm^{-1}. X-ray photoelectron spectroscopy (XPS) was performed by ESCALAB250 instrument (Thermo Fisher Scientific, East Grinstead, UK). XPS spectra were collected using a twin-crystal and micro-focusing monochromator, equipped with an Aluminium Kα X-ray source (1486.6 eV). X-ray diffraction (XRD) data were determined using D8 ADVANCE instrument (Bruker Co., Germany) equipped with Cu Kα radiation (λ = 1.5406 Å) at an accelerating voltage of 40 kV and an operating current of 100 mA. The diffraction intensities were detected in the range of 2θ = 5−90° with a scanning rate of 3°/min and step size of 0.02° at room temperature. The crystallinity index (CrI) was estimated according to the Segal method as the following equation [4, 5]:

$$CrI\ (\%) = \frac{I_{200} - I_{am}}{I_{200}} \times 100 \quad (1)$$

where I_{200} is the intensity of the diffraction peak at 2θ = 22.3°, and I_{am} is the intensity of the diffraction peak at 2θ = 18°.

The average crystalline domain size was calculated using the Debye-Scherrer equation [30, 31]:

$$D = \frac{K\lambda}{\beta cos\theta} \quad (2)$$

where K is the dimensionless shape factor (0.90), λ is the wavelength of radiation (λ = 1.5406 Å), β is the full width at the half maximum intensity of I_{200}, and θ is the diffraction angle of the (200) peak.

The structural morphologies of the isolated samples, CNFs, and fracture surface of the nanocomposites were examined by field emission scanning electron microscopy (FE-SEM, JSM−7600F, JEOL, Tokyo, Japan) at an accelerating voltage of 2.0−15.0 kV. The specimens were placed on the carbon tape and sputter-coated with a conductive layer of gold. Field emission transmission electron microscope (FE-TEM) micrographs of CNFs were observed by FE-TEM (JEM−2100F, JEOL, Tokyo, Japan) at an accelerating voltage of 200 kV. Thermogravimetric analysis (TGA) was measured using a Q50 Universal V20.13 Build 39 (TA instruments, New Castle, DE, USA) All samples were heated from 30 to 800 ℃ at a heating rate of 10 ℃/min under nitrogen atmosphere with a flow rate of 60 mL/min.

Tensile tests were performed on an ElectroPuls E3000, using a 5 kN load cell and a cross-head speed of 500 mm/min in accordance with ISO 37. Viscoelastic properties of the nanocomposites were measured by dynamic mechanical analysis (DMA) measurement using

Q850 (TA Instruments, USA). The DMA tests were conducted in tensile mode at 10 Hz and with a heating rate of 3°C/min. The water absorption was determined by immersing the samples in deionized water at room temperature for 14 days. After specific time intervals, the samples were removed, gently blotted with blotting papers, weighed using a four-digit balance, and soaked in deionized water again. The percentage of water absorption of each sample was calculated as follows:

$$Water\ absorption\ (\%) = \frac{M_t - M_0}{M_0} \times 100 \quad (3)$$

where M_t is the weight of the specimen at day t, and M_o is the initial weight of the specimen.

The crosslink density of the neat NR and the nanocomposites was determined by the equilibrium swelling method in toluene for 4 days. The samples were weighed and soaked in toluene under ambient conditions. The swollen samples were periodically taken out from the solvent, gently blotted with blotting papers, and weighed immediately. Cross-link densities (υ) were calculated by using the Flory−Rehner equation [32, 33]

$$\upsilon = \frac{\ln(1 - V_r) + V_r + \chi {V_r}^2}{V_1({V_r}^{1/3} + \frac{V_r}{2})} \quad (4)$$

where V_r is the volume fraction of the equilibrium swollen rubber:

$$V_r = \frac{\frac{m_r}{\rho_r}}{\frac{m_r}{\rho_r} + \frac{m_s}{\rho_s}} \quad (5)$$

V_1 and χ are the molar volume and interaction parameter of toluene (V_1 = 106.2 cm^3/mol, χ = 0.34). m_r and ρ_r are the weight and density of rubber in the sample. m_s and ρ_s are the weight and density of toluene (ρ_s = 0.865 g/cm^3), respectively.

4.0 RESULTS AND DISCUSSION

4.1 Surface Modification of BF, and Pretreated BFRP Composites

4.1.1 FT-IR spectra analysis

During alkali pretreatment, the acetate group from the hemicellulose will be removed. Thus hydrolytic enzymes can more easily access the carbohydrates, and it helps to remove lignin. Mercerization has been explained as an interdigitation of adjacent microfibrils with opposite polarities in fiber cell walls [34]. During the mercerization, the full fibers are converted into a swollen state, and the hydroxyl groups on the cellulose surface can interact with one another to form different types of intra- and inter-molecular hydrogen bonds. The NaOH content is adjusted according to the purpose, and the mechanical strength increases at specific content. FTIR studied the chemical structure and all spectra are normalized in Fig. 3. The FTIR spectra of all samples showed typical spectra of cellulose. The peaks in the range of 3,550 and 3,200 cm^{-1} are attributed to the –OH stretching band. In addition, three peaks, which are colored with

purple, are attributed to the acetyl group. The peak observed at 1,450 cm^{-1} can be ascribed to the CH_2 deformation in cellulose. Overall, the FTIR spectra for all samples were nearly identical, indicating that no new functional groups were added to the cellulose molecules. Mercerization made the fiber more hydrophilic, and the non-structural materials, such as hemicellulose, lignin, xylose, and other impurities, were partly removed after alkali treatment. In the acetylated BF, we can verify that specific absorption bands of the acetyl group at purple-colored peaks are increased compared with the untreated BF and decreased the OH group.

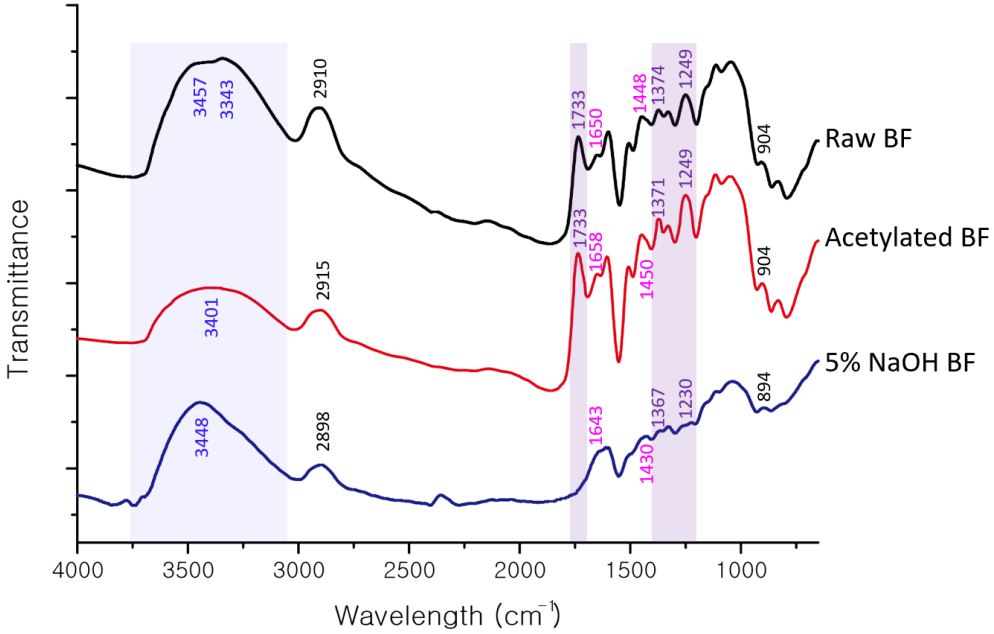

Figure 3. FTIR spectra of raw bamboo fiber and treated bamboo fiber in each method.

4.1.2 Structural Morphology

Reactive gas is an important factor in plasma treatment, and a suitable gas can effectively access into active functional groups and hence to improve the bonding performance [35]. After plasma treatment using C_4F_8 gas, whether functional groups were deposited by measuring the contact angle was confirmed. As shown in Fig. 4a, an appropriate value was found by treating plasma on an untreated bamboo panel and controlling the number of times the plasma beam reciprocates. When repeated about 5 times, the contact angle was confirmed to be 130°, and when repeated 10 times, the contact angle was the highest at 138°. There was no further increase in the contact angle when it was repeated more than 10 times. In Fig. 4c, the contact angle according to the NaOH content was compared when the number of plasma exposures was fixed at 10R. As the NaOH content increased, the contact angle decreased, and the contact angles of 2 wt% and 5 wt% NaOH treated bamboo panels were 123° and 120.3°, respectively, showing hydrophobicity, whereas in 15 wt% NaOH showed a hydrophilic tendency, with 83.5° of contact angle. As confirmed in Fig. 4b, the higher NaOH content, bamboo fibers showed a strong hydrophilic. For hydrophobization of fibers, NaOH treatment at a low content seems advantageous, but alkali treatment at a content of 5 wt% or less is not suitable for removing impurities, which is the original purpose of alkali treatment. Therefore, 5 wt% NaOH treated bamboo fiber was used for composite material synthesis in this study based on the reported research [36], and tensile testing was performed.

(a)

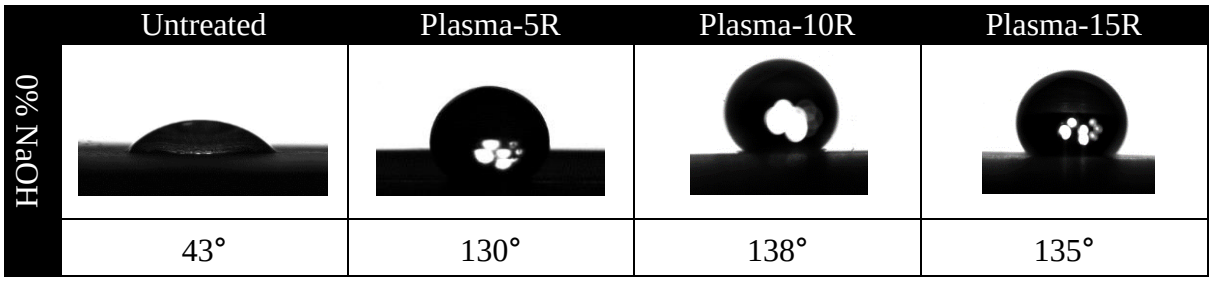

(b)

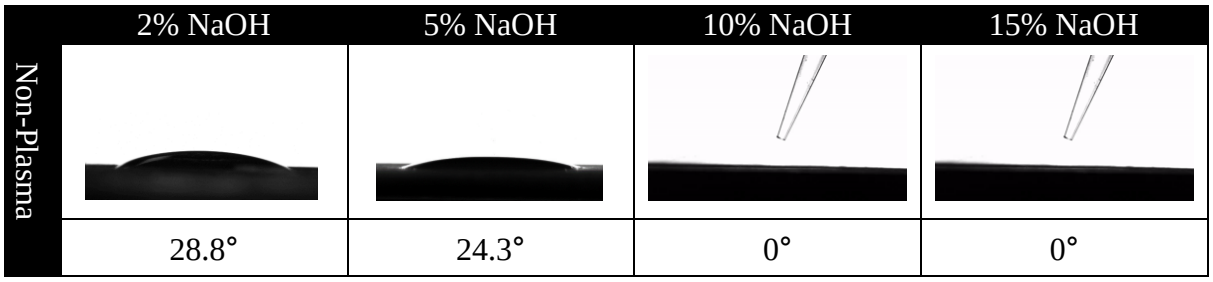

(c)

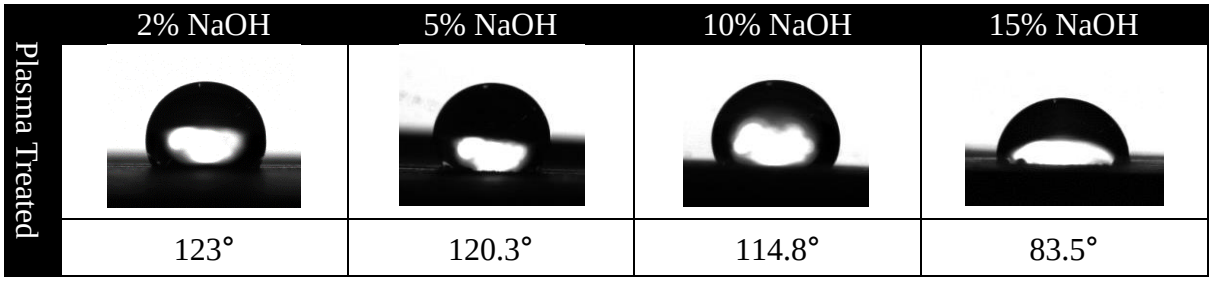

Figure 4. Before and after plasma treatment (a) Raw bamboo panel, (b−c) NaOH treated bamboo panel.

The structural morphology change of the bamboo fiber surface according to the plasma exposure time was observed As shown in Fig. 5a and b, it confirmed that the bamboo fibers were covered with lignin and impurities before plasma treatment. However, as the exposure time to the plasma gas increases, the impurities are gradually removed, and it seems to increase roughness on the bamboo fiber surface. The cracks and grooves on the fiber surface enlarge the interfacial area, which may cause improved adhesion by mechanical interlocking between bamboo fiber and matrix material. Rough surface topography and the higher surface area provided better interaction and mechanical interlocking between the fiber and polymer matrix, leading to the superior mechanical properties of the composite [36].

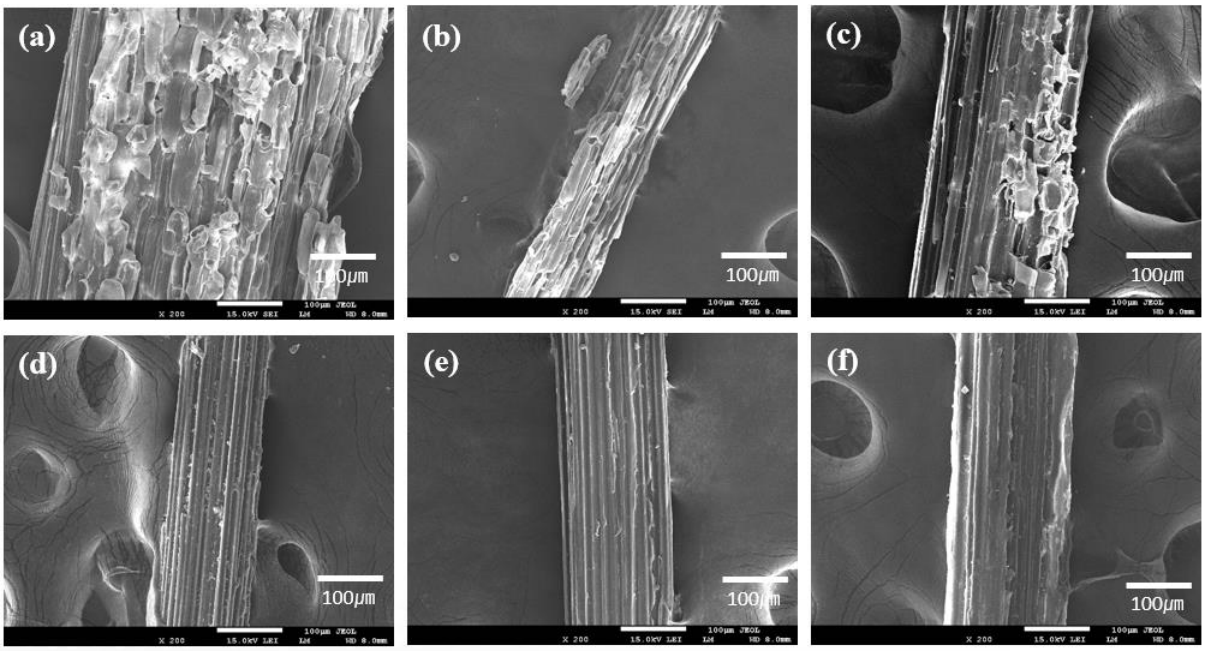

Figure 5. SEM micrographs for longitudinal section of (a) untreated bamboo fiber and (b) plasma-treated bamboo fiber (P-BF) for (c) 1 min, (d) 2 min, (e) 4 min, and (f) 5 min.

Fig. 6 shows the fracture surface of the BF/PLA composites, implying the interfacial adhesion between bamboo fibers and the PLA matrix. As shown in Fig. 6a, some agglomerated fibers were detected in untreated bamboo fibers, and the gap between the fibers and the matrix seems to show poor adhesion and dispersion. The black, long hole shown in Fig. 6b is where the bamboo fiber was extracted during the tensile test due to poor interfacial adhesion. It is considered as a result of weakening the bonding strength with the PLA matrix due to the increase in hydrophilicity by alkali treatment. On the other hand, the acetylated bamboo fiber has a small gap with the matrix and appears to have relatively good interfacial adhesion in Fig. 6c. The average length of the fibers was 4.74 mm after extraction by end-mill, but the diameter confirmed after synthesis was 0.61 mm, which was reduced by 87%. When the Haake rheomixer mixes the resin and the fiber during synthesis, the fibers are sheared off by shear stress, thereby shortening the fiber length. As a result, the average length of the chemically treated fibers was reduced by about 50% compared to the untreated bamboo fibers with alkalization of 0.3 mm and acetylation of 0.32 mm.

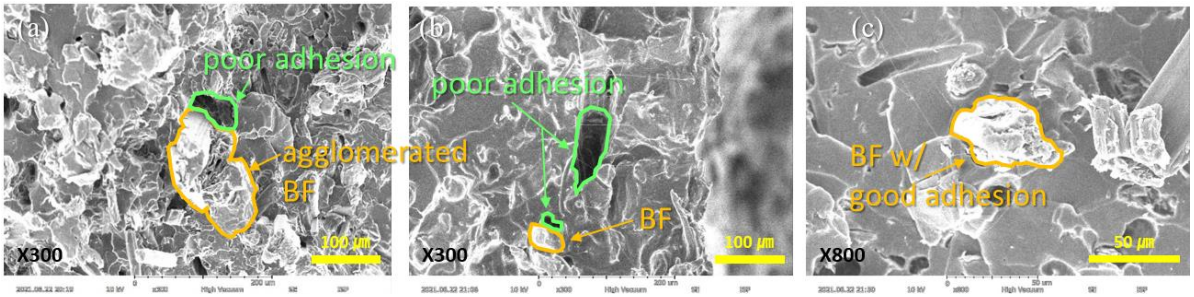

Figure 6. SEM micrographs for tensile fracture surface of (a) untreated BFRP, (b) 5% NaOH treated BFRP, and (c) acetylated BFRP.

4.1.3 Mechanical properties

The tensile behavior of BFRP was characterized by tensile testing of injection-molded samples. As was shown in Fig. 7, neat PLA abruptly broke after stress was applied without neck formation, characteristic of brittle material.

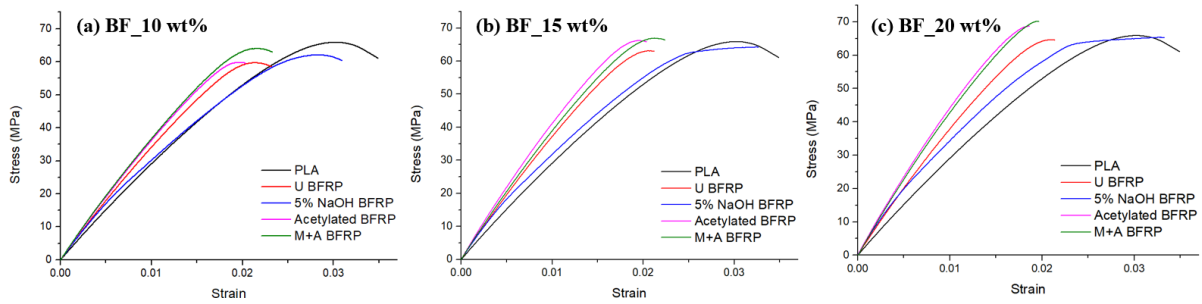

Figure 7. Stress-Strain curve of neat PLA and composites with (a) 10 wt.%, (b) 15 wt.%, and (c) 20 wt.% of bamboo fiber treated in each method.

Table 4 summarizes all tensile test results. All kinds of fiber surface modification had a positive effect on improving the modulus. As the fiber content increased, the tendency became more pronounced. In particular, the modulus of acetylated BFRP at 20 wt.% of BF was 4.5 GPa, which was improved by 53.6% compared to pure PLA. Tensile strength was improved with a slight difference from PLA at 15 wt.% or more bamboo content, except for alkali-treated BFRP. It results from the poor interfacial adhesion between bamboo fiber and PLA matrix due to increased hydrophilicity by alkali pretreatment.

Table 4. Mechanical properties of PLA and BFRP in each pre-treatment method.

	Fiber Weight Fraction (wt%)	**Tensile Strength (MPa)**	**Young's Modulus (GPa)**	**Elongation at Break**
PLA	-	65.21±2.20	2.93±0.12	3.35±0.51
Untreated BFRP	5	59.37±1.37	3.09±0.08	2.69±0.12
	10	59.80±1.07	3.39±0.08	2.34±0.03
	15	63.11±1.03	3.72±0.05	2.22±0.19
	20	64.60±0.93	3.88±0.04	2.18±0.11
Plasma Treated BFRP	5	60.36±2.05	3.20±0.11	2.97±0.22
5% NaOH Treated BFRP	10	61.95±1.17	3.01±0.06	3.26±0.17
	15	63.95±0.52	3.18±0.06	3.57±0.25
	20	66.02±0.54	3.49±0.06	3.74±0.20
Acetylated BFRP	10	59.67±1.90	3.61±0.09	2.17±0.14
	15	65.55±1.39	4.12±0.09	1.99±0.04

	20	68.05±2.92	4.50±0.07	1.81±0.11
5% NaOH + Acetylated BFRP (M+A BARP)	10	63.98±1.14	3.64±0.04	2.33±0.08
	15	66.89±0.52	3.93±0.05	2.21±0.07
	20	68.59±1.57	4.26±0.05	1.96±0.06

The C_4F_8 plasma treatment by atmospheric pressure plasma did not improve the physical and mechanical properties, shown in Table 4. It is due probably to that for C4F8 gas, the applied plasma power may not be intensive enough to produce excited state molecules and particles, and such cannot effectively alter the functional groups of the bamboo surface. Compared with untreated BFRP, a slight increase in the physical and mechanical properties may be due to the spark of plasma particles on the bamboo, producing rougher surfaces of bamboo bundles. The rough surface may give rise to an increase in the contact area of PLA resin and hence in the interface bonding of bamboo and PLA resin. There is a possibility that the external environment easily influences the unstable functional group in the excited state, and thus the duration is shortened.

4.2 Extraction of Cellulose Nanofibrils from BF

4.2.1 Compositional analysis

The chemical compositions of the fibers at each stage of treatment are summarized in Table 5. Raw bamboo fibers contain 36.76% cellulose, 28.33% hemicellulose, and 27.01% lignin. After chemical pretreatments and nanofibrillation process, the obtained CNFs contain 94.52% cellulose and 0.61% hemicellulose with no lignin detected. The percentage of cellulose increased significantly, while hemicellulose and lignin contents decreased effectively after each chemical pretreatment. Thus, the yield of CNF with respect to the raw bamboo fibers was 22.52%.

Table 5. Chemical compositions and yields of the fibers after different treatments.

Samples	**Cellulose (%)**	**Hemicellulose (%)**	**Lignin (%)**	**Residue yield (%)**
Raw bamboo fibers	36.76±1.14	28.33±2.76	27.01±0.12	-
Microwave-liquefied residues	61.37±0.71	20.53±0.61	10.66±1.13	35.17±0.81
Delignified fibers	73.55±0.34	18.10±1.49	0.74±0.06	26.73±2.10
Cellulose fibers	93.99±0.64	0.65±0.04	-	23.96±2.21
Cellulose nanofibrils	94.52±0.42	0.61±0.04	-	22.52±1.11

4.2.2 FTIR spectroscopy characterization

The FTIR spectra of all the samples are shown in Fig. 8a. The peak at 1,735 cm^{-1} is indicative

of the acetyl and uronic ester groups of hemicellulose and/or the ester linkage of carboxylic groups between ferulic acid and/or p-coumaric acid of lignin and hemicellulose. The peaks at 1,597, 1,511, 1,461, and 1,243 cm^{-1} are characteristic of the aromatic ring vibrations, C−H deformations combined with C=C vibrations of lignin, and/or methoxyl groups of lignin [37-39]. All the above peaks could be seen in the spectrum of raw bamboo fibers. The intensity of the peak at 1,735 cm^{-1} decreases after microwave liquefaction, corresponding to the cleavage of ester bonds between lignin and carbohydrate (REF). The disappearance of the intensity peak at 1,735 cm^{-1} in the spectrum of CFs can indicate the effective removal of hemicellulose. It was also observed in the spectra of microwave-liquefied residues that the peak at 1,597 cm^{-1} disappeared while the peaks at 1,511, 1,461, and 1,243 cm^{-1} became very small shoulders. After HPAC treatment, lignin was completely removed through the absence of lignin peaks in the spectrum of the delignified fibers. The small shoulder band at 1,209 cm^{-1} corresponds to the S=O vibration of sulfate half ester groups attached to the fibers during the microwave liquefaction and acid hydrolysis. The peaks appeared at 1,167, 1,114, and 1,032 cm^{-1} due to the C−O−C stretching vibrations of the β-1,4-glycosidic ring linkages between the D-glucose units in cellulose. Also, the shoulder peak seen in the region of 897 cm-1 corresponds to the C1−H glycosidic deformation of cellulose [40].

4.2.3 Crystal structure analysis

X-ray diffractograms of all the samples are given in Fig. 8b. All the samples show similar XRD patterns with four diffraction peaks at 2θ = 14.6 °, 16.3 °, 22.3 °, and 34.5 °, corresponding to the (1−10), (110), (200), and (004) crystalline planes of cellulose I lattice [41,42]. In raw bamboo fibers, the crystalline domains are closely bound with the matrix of lignin and hemicellulose, leading to a low CrI (62.38%). It is noted that the increment in the CrI values can be further seen in the XRD spectra of microwave-liquefied residues (78.08%), delignified fibers (78.46%), CFs (78.62%), and CNFs (80.82%), respectively. The average crystalline domain size of all the samples is shown in Table 8, indicating an increasing trend from 5.61 nm to the highest value of 6.49 nm. This is mainly because the effective removal of non-cellulosic components promoted the rearrangement of the cellulosic chains through hydrogen bonding. These chains are organized and packed closely together, forming highly ordered zones, and giving rise to the greater crystallinity index as well as the crystalline size.

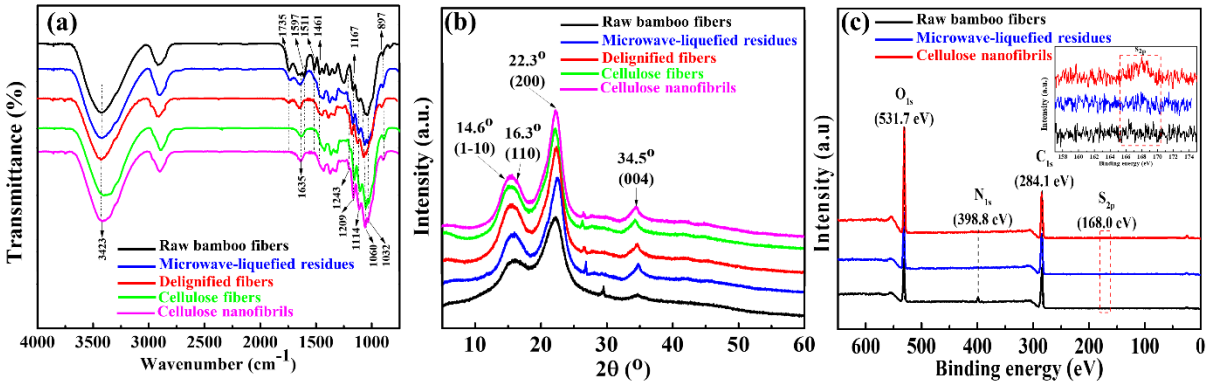

Figure 8. (a) FTIR spectra, (b) XRD patterns, and (c) XPS spectra of the samples.

4.2.4 Elemental composition analysis

XPS survey spectra of the samples are presented in Fig. 1c, while Table 6 summarizes the surface elemental compositions of these materials. The increase of the O/C ratio can mainly be attributed to the effective removal of lignin and hemicellulose from biomass. Another explanation could be due to the structure of lignin mainly containing crosslinked phenolic polymers with a high percentage of carbon. The elimination of lignin decreased the carbon content and increased the O/C ratio. The presence of the new peak at 168.0 eV can indicate S2p-binding energy. The high-resolution C1s and O1s scans of the samples are shown in Fig. 9. The C1 peak represents C−C/C−H, while the C2 peak relates to carbon atoms in the presence of ether groups (C−O−C) and the unmodified C−OH groups of cellulose chains. The C3 peak indicates the contribution of acetal moieties of the anhydroglucose units and/or ester groups relating to hemicellulose and lignin [43]. The effective removal of lignin and hemicellulose resulted in the decrease in the intensity of the C1 and C3 peaks. In contrast, the increase in the intensity of the C2 peak could be seen as a result of the accommodation of cellulose components after chemical treatments. The O1 peak indicates oxygen atoms (O−C=O) from lignin and/or hemicellulose structure, whereas the O2 peak relates to oxygen atoms bonded to carbon (C−O−C and C−O) from lignin, hemicellulose, and cellulose in raw bamboo fibers. From the results of the O1s spectra, the O1 peak decreased, whereas the O2 peak strengthened after each chemical treatment.

Table 6. Surface element compositions of raw bamboo fibers, microwave-liquefied residues, and cellulose nanofibrils.

Samples	O_{1s} (%)	C_{1s} (%)	N_{1s} (%)	S_{2p} (%)	O/C
Raw bamboo fibers	25.39	70.30	4.31	-	0.36
Microwave-liquefied residues	29.19	70.53	-	0.28	0.41
Cellulose nanofibrils	40.72	58.85	-	0.43	0.69

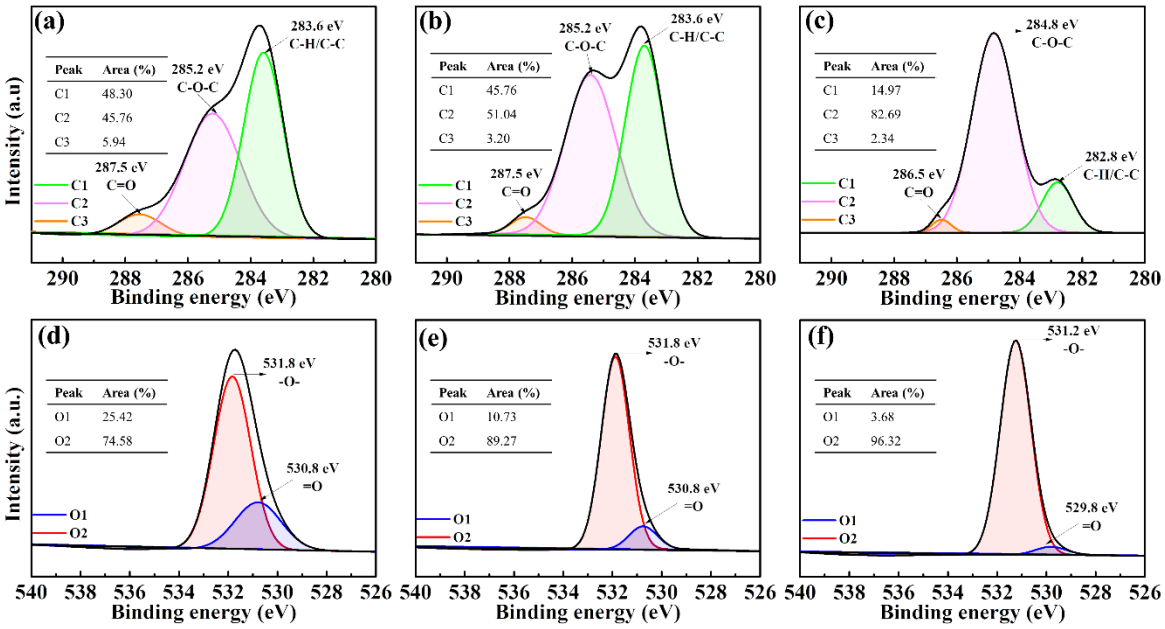

Figure 9. High-resolution C1s and O1s spectra of the samples.

4.2.5 Morphological characterization

The morphologies of all the samples are observed in SEM micrographs. It can be seen from Fig. 10a−b that the raw bamboo fibers exhibit numerous fiber bundles and aggregates with the presence of small fragments on the surface. The surface morphology of microwave-liquefied residues demonstrates intact structure with the rough surface (Fig. 10c−d). These images indicate that the cementing components, such as lignin, hemicellulose, and extractives, connecting with cellulose in raw bamboo fibers, were effectively removed. Notably, HPAC and alkaline pretreatments seem to be the effective way to open and separate the fiber bundles into microfibrils (Fig. 10e−f). Each microfibril can be supposed as a bundle of nano-sized fibrils attached along the microfibrils by amorphous zones. The TEM images seen in Fig. 4a can indicate that CNFs show a wire-like nanofibrils structure with some aggregates. The TEM images can also show that the nanofibrils are entangled together, forming an interconnected network. The intertwined arrangements of nanofibrils could provide a great reinforcing efficiency in composite applications. The calculated size distribution histogram of CNFs (Fig. 11b) reveals that the majority of the nanofibrils have an overall cross-sectional diameter of 5−30 nm with an average diameter of 13 nm.

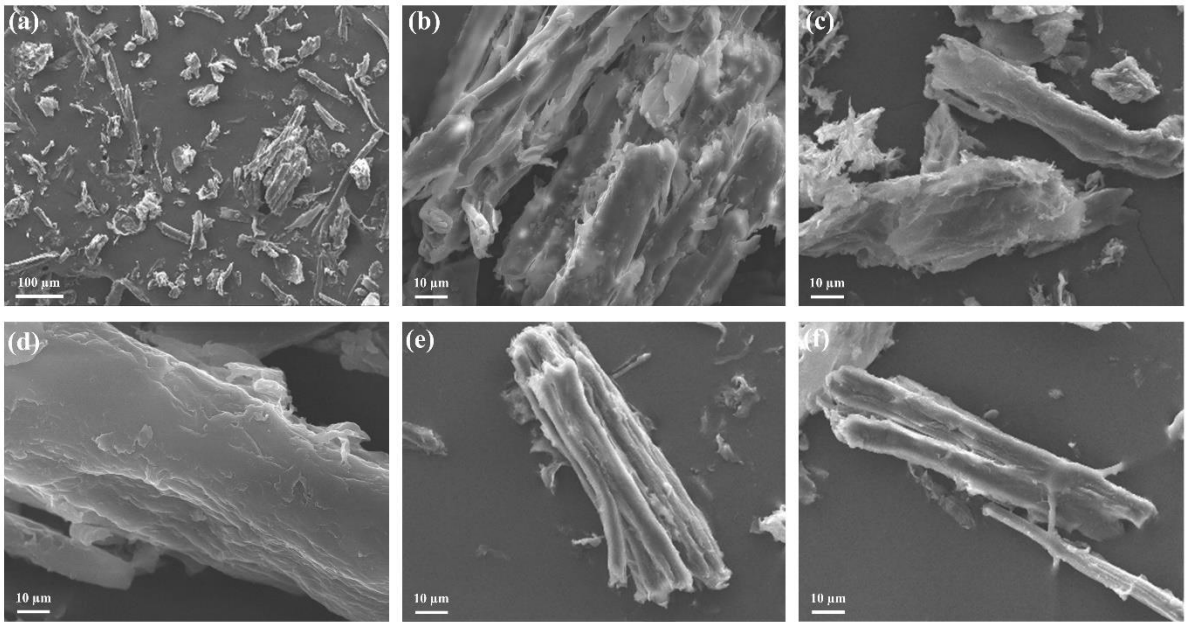

Figure 10. SEM images of (a−b) raw bamboo fibers, (c−d) microwave-liquefied residues, (e) delignified fibers, and (f) cellulose fibers.

4.2.6 Thermogravimetric analysis

The thermal performances of all the samples are shown in Fig. 4c−d. TGA curve of raw bamboo fibers displays mainly two steps of thermal decompositions. The first step of the degradation occurred between 226 and 400℃, corresponding to the carbohydrate degradation and the onset of lignin degradation. The second step occurred around 400−700℃, corresponding to lignin residues [44, 45]. All the samples show a small weight loss when heated from 50 to 150℃. This is likely because of the vaporization of absorbed-bound water. The raw bamboo fibers started decomposition at 226℃, while the microwave-liquefied residues and the delignified fibers decomposed at 265 and 269℃, respectively. The higher onset temperature indicates that hemicellulose and lignin recognized as lower thermally stable materials in the

early stage of the decomposition were efficiently removed. Furthermore, a similar trend can be seen in the T_{max} value of the residues after microwave liquefaction (365℃) when compared to raw bamboo fibers (346℃). However, there is a decrease in the T_{max} value of delignified fibers (310℃), CFs (307℃), and CNFs (305℃). This result can be explained by the fact that HPAC treatment played a role in the disintegration of the fiber bundles into individual microfibrils and the increment of the heat capability to attack the fibers, thereby resulting in the decrease in the T_{max}. Another explanation can be because the introduction of sulfate groups during liquefaction and acid hydrolysis developed the dehydration reactions, thereby resulting in the decrease in activation energy of the degradation and lowering the thermal stability of the fibers [46-48].

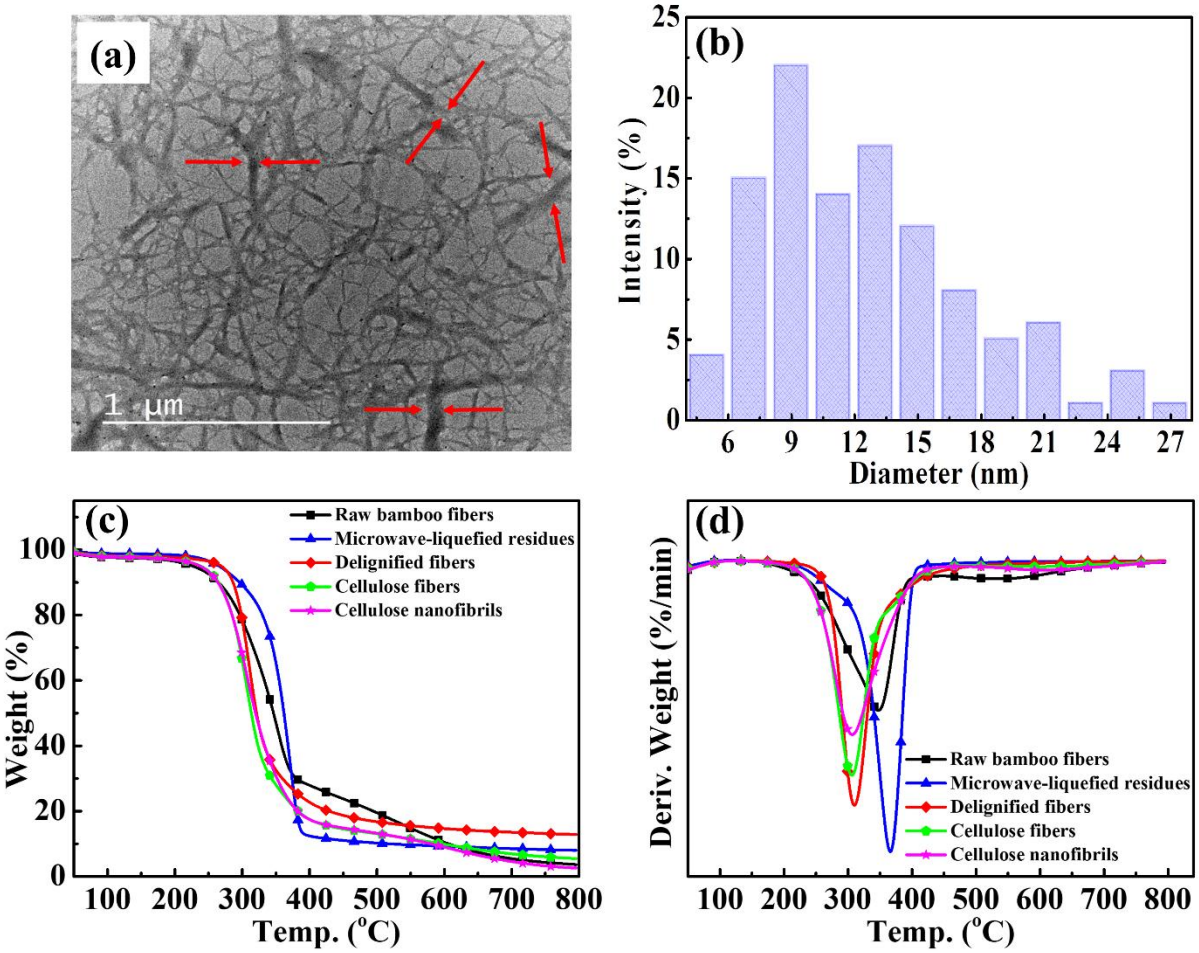

Figure 11. (a) TEM image of CNFs, (b) diameter distribution of CNFs, (c) TG curves, and (d) DTG curves of the samples.

4.3 Characterization of NR/CNFs Bio-composites

4.3.1 Tensile properties

The stress-strain curves of neat NR and NR/CNFs bio-composites are shown in Fig. 12a. The tensile properties of bio-composites include tensile strength, modulus at 50% strain, elongation at break, and work-of-fracture, which are summarized in Table 7 with the CNFs loading of 5 phr, the tensile strength significantly increased from 10.18 to 19.55 MPa. The tensile strength of NR/CNF10 and NR/CNF15 was found to be 22.48 and 20.75 MPa, respectively. Although

the inherently poor interfacial interactions between the matrix and the filler, the addition of unmodified CNFs in the NR matrix resulted in a significant improvement in tensile properties as compared to the neat NR. The utilization of the latex mixing process helped in the well-dispersion of CNFs in the NR matrix without using any coupling agents. The incorporation of CNFs restricted the mobility of the polymer chains leading to increased tensile strength and modulus values. It could further explain that the formation of Zn/CNF and CNF/CNF three-dimensional networks also played an important role in the enhancement of the tensile properties of the bio-composites. However, the agglomeration could happen at the high filler loading, leading to a reduction in the matrix-filler interaction and a decrease in the mechanical properties of the NR/CNF15 sample. The elongation at break of NR/CNF5 also increases from 398 to 454% compared to the neat NR. The NR/CNF10 and NR/CNF15 samples exhibit the elongation at break values of 523 and 504%, respectively. The work-of-fracture (toughness) value is proportional to the area under the stress-strain curve, which increased 1.8 to 2.4 times higher when compared to the neat NR. Since toughness is expressed to be the material's resistance to fracture (or the energy needed to cause fracture), the enhancement of toughness should be directly associated with the formation of the percolating network, which played a vital role in the distribution of the applied stress through the whole hybrid bio-composites in order to prevent the fracture. Overall, the increments in mechanical properties of hybrid bio-composites reinforced with CNFs are the results from load sharing of CNFs and the NR matrix. The formation of percolated CNFs networks also played an important role in the property increases.

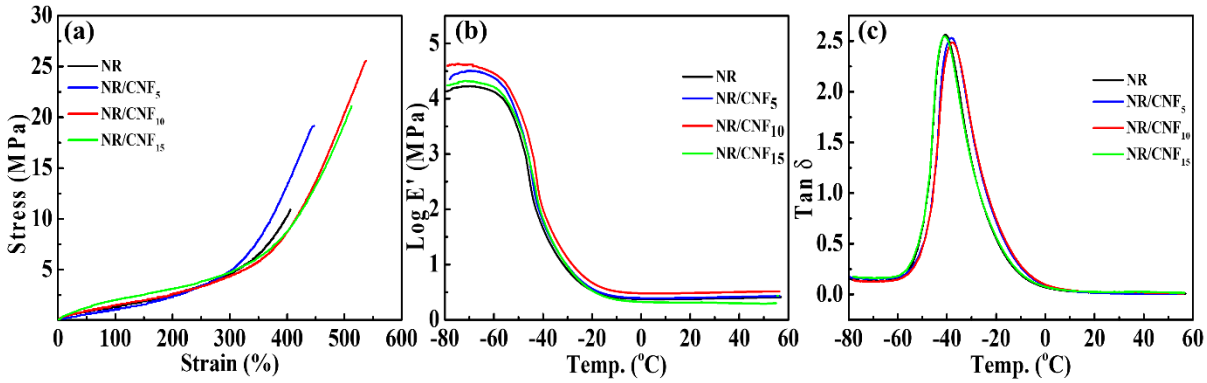

Figure 12. (a) Tensile stress−strain curves, (b) Logarithm storage modulus vs. temperature plots, and (c) Tan delta vs. temperature plots of the neat NR and its nanocomposites.

Table 7. Tensile test data of the bio-composites.

Sample	Tensile strength (MPa)	Modulus at 50% (MPa)	Elongation at break (%)	Work-of-fracture (MJ/m^3)
NR	10.18 ± 1.37	1.38 ± 0.20	398 ± 10	1.22 ± 0.15
NR/CNF_5	19.55 ± 1.04	1.13 ± 0.03	454 ± 6	2.19 ± 0.11
NR/CNF_{10}	22.48 ± 2.80	1.52 ± 0.02	523 ± 16	2.92 ± 0.45
NR/CNF_{15}	20.75 ± 0.32	2.30 ± 0.07	504 ± 16	2.78 ± 0.17

4.3.2 Dynamic mechanical analysis

Fig. 12b shows the plots of the logarithm storage modulus (log E') versus the temperature of

the neat NR and the NR/CNFs bio-composites. Both composites show an increase in the storage modulus in the glassy region than the neat NR, while the NR/CNF10 sample indicates the highest value. The incorporation of CNFs enhanced the stiffness of the composites in the glassy state in which the polymer chains motions are largely restricted. At around -60°C, a sharp drop in the storage modulus could be seen for all the samples, corresponding to the glass transition region. After the sharp decrease, the modulus remains almost constant in the rubbery plateau region over the long temperature range. The storage modulus at 25°C of the neat NR, NR/CNF5, NR/CNF10, and NR/CNF15 are 2.42, 2.52, 3.09, and 2.05 MPa, respectively. Fig. 12c shows the loss tangent (tan δ) curves of the neat NR and the composites with temperature variation. Tan δ curves of all the samples show the maximum values corresponding to the glass transition temperature (T_g). The T_g of the neat NR, NR/CNF5, NR/CNF10, and NR/CNF15 are -40.44, -38.20, -37.88, and -40.77°C, respectively (Table 8). Although these values are not significantly different, the incorporation of CNFs resulted in the slight, positive shift in T_g value toward the higher temperature, indicating the strong interaction between the matrix and the filler. The tan δ peak height of the neat NR, NR/CNF5, NR/CNF10, and NR/CNF15 are 2.56, 2.53, 2.49, and 2.55, respectively. At the matrix/filler interface, the rubber chains' movements are possibly hindered, which is responsible for the reduction in the magnitude of the tan δ peak of the composites compared to the neat NR.

Table 8. DMA data of the bio-composites.

Properties	**T_g (°C)**	**Maximum tan δ**
NR	-40.44	2.56
NR/CNF_5	-39.46	2.62
NR/CNF_{10}	-37.88	2.49
NR/CNF_{15}	-40.70	2.55

4.3.3 Physical properties

It is well-known that the physical properties of the neat NR and its bio-composites strongly depend on the inclusion of the filler into the rubber matrix. As summarized in Table 9, the apparent density of the neat NR is 0.9421 g/cm^3, while the NR/CNF15 composite indicates the highest value of 0.9861 g/cm^3. The density values of the composites also increased with the increase of the filler loadings. During the latex mixing, CNFs are well-dispersed in the matrix, thus restricting the aggregation of CNFs. Meanwhile, the amphipathic protein molecules in the NR latex might have hydrogen bonding interactions with CNFs, which helped in the uniform distribution of the filler in close contact with the matrix. In the following coagulation process, the rubber particles precipitated and formed excluded interspaces. The addition of CNFs decreased the interspace volume, leading to the formation of the compact composite structure, and then responsible for the increase in the density.

Table 9. Apparent density, toluene adsorption percentage, and crosslink density of the NR/CNFs bio-composites.

Properties	**Apparent density (g/cm^3)**	**Toluene absorption percentage (%)**	**Cross-linking density × 10^{-4} (mol/cm^3)**
NR	0.9421 ± 0.0042	261 ± 4	2.41 ± 0.07
NR/CNF_5	0.9507 ± 0.0038	242 ± 7	2.58 ± 0.10
NR/CNF_{10}	0.9707 ± 0.0019	189 ± 2	3.43 ± 0.05
NR/CNF_{15}	0.9861 ± 0.0019	214 ± 4	2.96 ± 0.10

The degree of water absorption of bio-composites could be seen as a function of time and filler loading, which is shown in Fig. 6a. Most of all samples exhibit a rapid absorption in the first two days, and then the water uptake slowly increases until 14 days. As expected, the water uptake of the neat NR is low due to the inherent hydrophobicity of the polymer chains. Meanwhile, the hydrophilic origin of CNFs is the reason for the water absorption improvement through the formation of hydrogen bonds with water molecules. Thus, the higher loadings of the filler are the higher water absorption of the composites.

Toluene absorption behavior of all the samples shown in Fig. 13b gives evidence of the interaction between CNFs filler and NR matrix. The solvent uptake of the composites is lower than the neat NR, corresponding to the good matrix-filler interaction. The crosslink density summarized in Table 9 can be calculated from the equilibrium swelling tests by applying the Flory−Rehner equation. It is found that the composites exhibit a higher crosslink density compared to the neat NR. This could be explained that the uniform distribution of the filler in the rubber through the latex coagulation process as well as the polarity nature of CNFs hindered the penetration of toluene into the matrix, which resulted in the low value of toluene absorption and the high value of the crosslink density.

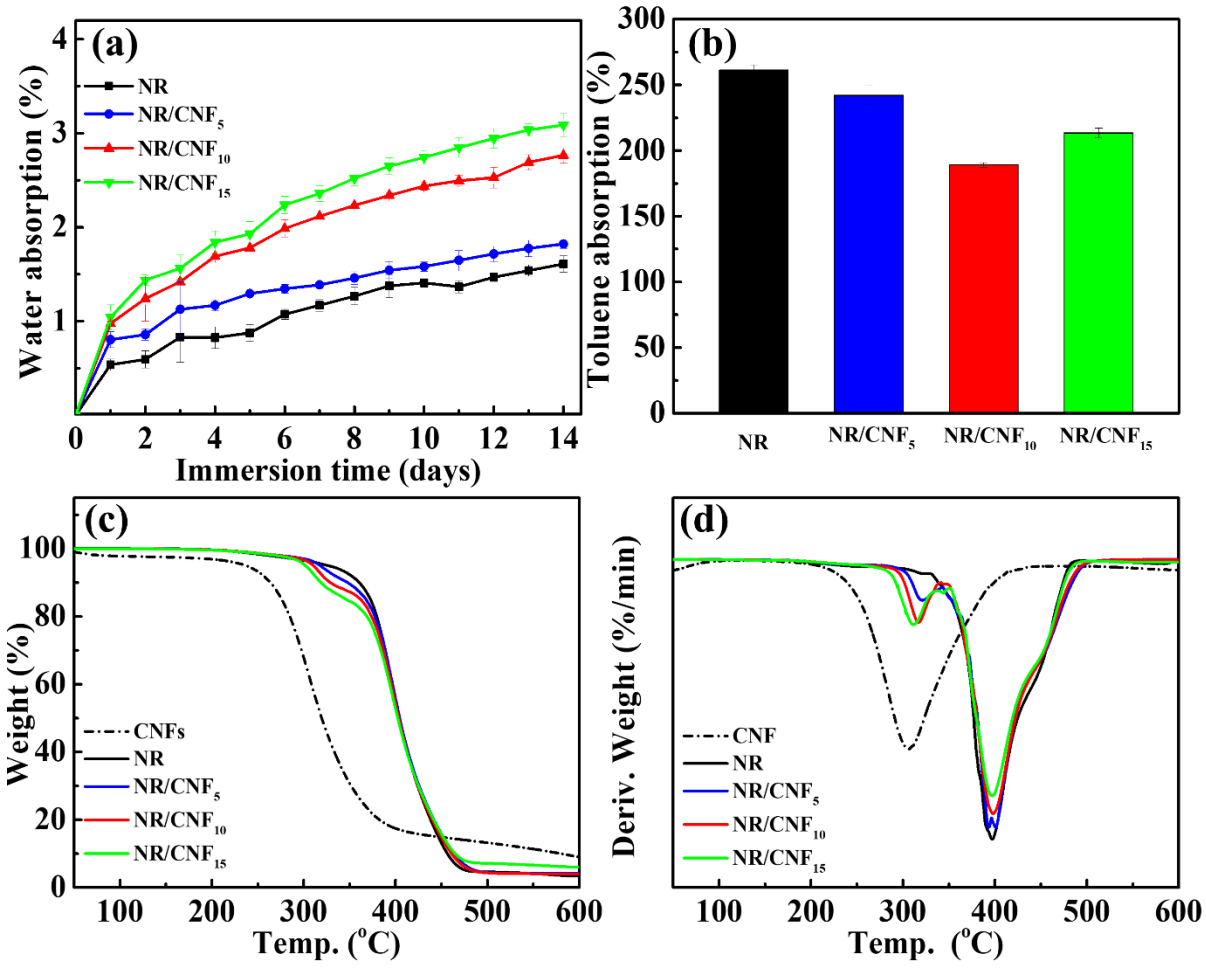

Figure 13. (a) Water absorption, (b) toluene absorption, (c) TG curves, and (d) DTG curves of the NR/CNFs bio-composites.

4.3.4. Thermogravimetric analysis

The thermal behavior of CNFs, NR, and its bio-composites was investigated by TGA, which is shown in Fig. 13b−c. Table 10 summarizes the TGA data, including the 5% weight loss (T_5), 10% weight loss (T_{10}), 50% weight loss (T_{50}), and charred residues at 600℃. The thermal decomposition of CNFs occurred between 237 and 400℃, whereas NR started its thermal degradation at higher temperature (327℃). The onset degradation temperature of NR/CNF5, NR/CNF10, and NR/CNF15 are 318, 310, and 302℃, respectively. The onset degradation temperature of the composites shifted to a lower temperature than the neat NR because the filler has lower thermal stability in the initial stage of decomposition. The higher loadings of CNFs resulted in the decrease of the onset degradation temperature, which could be seen in the T_5 and T_{10} values. The temperature of the 50% weight loss of the neat NR and the composites is not significant. The residues at 600℃ of CNFs and NR are 11.37% and 3.37%, respectively. Therefore, the filler itself has better thermal stability than the rubber at higher temperatures. The higher loadings of CNFs resulted in the higher char residue contents of the composites at the end of the thermogravimetric analysis.

Table 10. TGA data of the NR/CNFs bio-composites.

Samples	**T_5 (℃)**	**T_{10} (℃)**	**T_{50} (℃)**	**Residue at 600 ℃ (%)**
CNF	237	264	320	11.37
NR	327	361	404	3.37
NR/CNF_5	318	348	405	4.18
NR/CNF_{10}	310	329	404	4.03
NR/CNF_{15}	302	319	402	6.05

5.0 CONCLUSIONS

5.1 Surface Modification of Bamboo Fiber for Composites.

Mercerization, well-known as a traditional alkali treatment method, effectively removes impurities on the lignocellulose fiber, such as lignin and hemicellulose. However, the interfacial adhesion with polymers is relatively poor due to increased hydrophilicity. Therefore, the modulus value showed only 19% improvement compared to pure PLA at 20% bamboo content standard, and the tensile strength increased by 1.24%, confirming that it was at a similar level to PLA. In order to overcome the poor interfacial adhesion between the bamboo fibers and the PLA matrix, the hydrophobicity of fibers was increased by acetylation, and the modulus value was significantly improved to 53.6%. The tensile strength of the fibers to which both mercerization and acetylation were applied were improved by a slight difference compared to acetylated BFRP, but it is considered insignificant. In order to reduce the use of chemicals and minimize the process, acetylation alone is deemed to be sufficient to achieve the desired properties. However, since acetylation makes fibers brittle, to apply it to additive manufacturing, the use of an appropriate plasticizer is required to increase elongation, and additional research is needed. In introducing atmospheric pressure plasma for another fiber surface modification, using C_4F_8 gas in the pre-experiment (contact angle test), functional groups were given to the bamboo panel, and a contact angle of 138° was achieved. It confirmed the potential for future use to reduce the surface energy on the bamboo fiber.

5.2 Extraction of Cellulose Nanofibrils from Bamboo and NR/CNFs bio-composites

In summary, CNFs were successfully isolated from bamboo using microwave liquefaction combined with HPAC delignification, alkaline treatment, acid hydrolysis, and low energy

nanofibrillation. The chemical composition analysis confirmed that the green extraction method listed above was effectively eliminated the noncellulosic components from bamboo. The obtained CNFs contain 94.52% cellulose and 0.61% hemicellulose with no lignin detected and a yield of 22.52%. The chemical and morphological structures of the samples at each stage of treatments were further investigated using various analytical techniques like FTIR, XPS, TGA, and SEM. The crystalline structure of CNFs was characterized by XRD studies, indicating a high CrI of 80.82%. TEM observation indicated wire-like CNFs with the diameter range of 5−30 nm and the average diameter of 13 nm. NR/CNF nanocomposites were formed by the addition of CNFs into the rubber matrix, using latex mixing, compound mastication, and vulcanization. The tensile strength, toughness, and cross-link density values were found to be highest for the NR/CNF_{10} sample. The DMA analysis indicated that the addition of CNFs increased the storage modulus of the nanocomposites at the glassy state and the rubbery state. However, the T_g values of the nanocomposites were not significant. The fractographic studies show that CNFs were uniformly distributed in the rubber matrix, resulting in the effective stress transfer effects in the nanocomposites. Consequently, the presented results concluded that the obtained CNFs seem to be potential green reinforcements for NR-based nanocomposites without any surface modification needed.

5.3 Future plan

Optimal fiber length and diameter, engineering of interfacial strength bamboo fibers and polymer matrix, and viscosity control will be investigated to optimize the capability of 3D printing manufacturing. We will also optimize the 3D printing parameters, including printing speed, layer thickness, bed temperature, printing trajectory, and nozzle size. In addition, we will build a conventional core structure such as a honeycomb structure and evaluate the performance of the sandwich composite structure.

6.0 DELIVERABLES

- Conference Publications

: E. Oh, Tran Trung Tien, J. Shur, “Plasma surface treatment to improve the mechanical properties of eco-friendly composites”, *The Korean Society for Composite Materials, Fall Conference* (2020)

: E. Oh, Tran Trung Tien, J. Shur, “Effect of fiber pretreatment on mechanical properties of bamboo fiber reinforced polymer (BFRP) composites”, *The Korean Society for Composite Materials, Fall Conference* (2021)

- Journal Publications

: Tan Binh Nguyen, S. Hong, B. Yoon, J. Yoo, C. Kim, E. Oh, J. Suhr, "Cellulose nanofibrils extracted from bamboo as green reinforcing fillers for natural rubber nanocomposites”, *Polymer,* (2021) Under review.

- Joint Research Project

: w/ Science and Technology Park (STeP), Chiang Mai University “Development of Reinforcing Materials in Concrete by Natural Fiber Bars” *Thai government*, 2021~2024 (3 years, 250,000 USD)

7.0 REFERENCES

1. Deepa, B., et al. "Structure, morphology and thermal characteristics of banana nano fibers

obtained by steam explosion." Bioresource technology 102.2 (2011): 1988-1997.

2. Xu, Junming, et al. "Renewable chemical feedstocks from integrated liquefaction processing of lignocellulosic materials using microwave energy." Green Chemistry 14.10 (2012): 2821-2830.

3. Chirayil, Cintil Jose, et al. "Isolation and characterization of cellulose nanofibrils from Helicteres isora plant." Industrial Crops and Products 59 (2014): 27-34.

4. Chen, Wenshuai, et al. "Individualization of cellulose nanofibers from wood using high-intensity ultrasonication combined with chemical pretreatments." Carbohydrate Polymers 83.4 (2011): 1804-1811.

5. Dufresne, Alain, Jean-Yves Cavaillé, and Michel R. Vignon. "Mechanical behavior of sheets prepared from sugar beet cellulose microfibrils." Journal of applied polymer science 64.6 (1997): 1185-1194.

6. López, Joan Pere, et al. "Mean intrinsic tensile properties of stone groundwood fibers from softwood." BioResources 6.4 (2011): 5037-5049.

7. Vasuki, Yathunanthan, et al. "Semi-automatic mapping of geological Structures using UAV-based photogrammetric data: An image analysis approach." Computers & Geosciences 69 (2014): 22-32.

8. Cherian, B. M., A. L. Leão, and T. H. O. M. A. S. SF DE SOUZA. "S., POTHAN, LA, KOTTAISAMY, M." Carbohydrate Polymers 81 (2010): 720.

9. Tao, Peng, et al. "Enzymatic pretreatment for cellulose nanofibrils isolation from bagasse pulp: transition of cellulose crystal structure." Carbohydrate polymers 214 (2019): 1-7.

10. Kemp, Karen, et al. "An exploration of the follow-up up needs of patients with inflammatory bowel disease." Journal of Crohn's and Colitis 7.9 (2013): e386-e395.

11. Huang, Chih-Feng, et al. "Dual-functionalized cellulose nanofibrils prepared through TEMPO-mediated oxidation and surface-initiated ATRP." Polymer 72 (2015): 395-405.

12. Narendar, R., and K. Priya Dasan. "Chemical treatments of coir pith: morphology, chemical composition, thermal and water retention behavior." Composites Part B: Engineering 56 (2014): 770-779.

13. Jayabal, S., et al. "Effect of soaking time and concentration of NaOH solution on mechanical properties of coir–polyester composites." Bulletin of Materials Science 35.4 (2012): 567-574.

14. Liu, Yanping, and Hong Hu. "X-ray diffraction study of bamboo fibers treated with NaOH." Fibers and Polymers 9.6 (2008): 735-739.

15. Liu, Dagang, et al. "Bamboo fiber and its reinforced composites: structure and properties." Cellulose 19.5 (2012): 1449-1480.

16. Li, Xue, and G. L. Tabil. "Panigrahi S." Chemical Treatments of Natural Fiber for Use in Natu-ral Fiber-Reinforced Composites: A Review Journal of Polymers and the Environment 15.1 (2007): 25-33.

17. Chen, Hong, et al. "Effect of alkali treatment on wettability and thermal stability of individual bamboo fibers." Journal of Wood Science 64.4 (2018): 398-405.

18. Kabir, M. M., et al. "Chemical treatments on plant-based natural fibre reinforced polymer composites: An overview." Composites Part B: Engineering 43.7 (2012): 2883-2892.

19. Izani, MA Norul, et al. "Effects of fiber treatment on morphology, tensile and thermogravimetric analysis of oil palm empty fruit bunches fibers." Composites Part B: Engineering 45.1 (2013): 1251-1257.

20. Senthilkumar, K., et al. "Effect of alkali treatment on mechanical and morphological properties of pineapple leaf fibre/polyester composites." Journal of Polymers and the Environment 27.6 (2019): 1191-1201.

21. Phuong, Nguyen Tri, Cyrille Sollogoub, and Alain Guinault. "Relationship between fiber chemical treatment and properties of recycled pp/bamboo fiber composites." Journal of Reinforced Plastics and Composites 29.21 (2010): 3244-3256.

22. Li, Xue, Lope G. Tabil, and Satyanarayan Panigrahi. "Chemical treatments of natural fiber for use in natural fiber-reinforced composites: a review." Journal of Polymers and the Environment 15.1 (2007): 25-33.

23. Saheb, D. Nabi, and Jyoti P. Jog. "Natural fiber polymer composites: a review." Advances in Polymer Technology: Journal of the Polymer Processing Institute 18.4 (1999): 351-363.

24. Paul, Wambua, Ivens Jan, and Verpoest Ignaas. "Natural fibers: can they replace glass in fiber reinforced plastics." Compos Sci Technol 63.9 (2003): 1259-1264.

25. Bledzki, A. K., and Jochen Gassan. "Composites reinforced with cellulose based fibres." Progress in polymer science 24.2 (1999): 221-274.

26. Sahin, H. T., et al. "Surface fluorination of paper in CF 4-RF plasma environments." Cellulose 9.2 (2002): 171-181.

27. Ogawa, K., et al. "Quality control of fibers end-milled from bamboo pipe using spiral tool path." WIT Transactions on The Built Environment 85 (2006).

28. Onyekwere, O. S., A. C. Igboanugo, and T. B. Adeleke. "Optimisation of acetylation parameters for reduced moisture absorption of bamboo fibre using Taguchi experimental design and genetic algorithm optimisation tools." Nigerian journal of technology 38.1 (2019): 104-111.

29. John, Maya Jacob, and Rajesh D. Anandjiwala. "Recent developments in chemical modification and characterization of natural fiber-reinforced composites." Polymer composites 29.2 (2008): 187-207.

30. Chandra, Julie, Neena George, and Sunil K. Narayanankutty. "Isolation and characterization of cellulose nanofibrils from arecanut husk fibre." Carbohydrate polymers 142 (2016): 158-166.

31. Nagarajan, K. J., A. N. Balaji, and N. R. Ramanujam. "Extraction of cellulose nanofibers from cocos nucifera var aurantiaca peduncle by ball milling combined with chemical treatment." Carbohydrate polymers 212 (2019): 312-322.

32. Flory, Paul J., and John Rehner Jr. "Statistical mechanics of cross-linked polymer networks I. Rubberlike elasticity." The journal of chemical physics 11.11 (1943): 512-520.

33. Cao, Liming, Jiarong Huang, and Yukun Chen. "Dual cross-linked epoxidized natural rubber reinforced by tunicate cellulose nanocrystals with improved strength and extensibility." ACS sustainable chemistry & engineering 6.11 (2018): 14802-14811.

34. Okano, T., and A. Sarko. "Mercerization of cellulose. II. Alkali–cellulose intermediates and a possible mercerization mechanism." Journal of Applied Polymer Science 30.1 (1985): 325-332.

35. Rao, Jiuping, et al. "Plasma surface modification and bonding enhancement for bamboo composites." Composites Part B: Engineering 138 (2018): 157-167.

36. Zhang, Kai, et al. "Thermal and mechanical properties of bamboo fiber reinforced epoxy composites." Polymers 10.6 (2018): 608.

37. Chandra, J., et al. “Isolation and characterization of cellulose nanofibrils from arecanut husk fibre.” Carbohydrate Polymers 142 (2016): 158−166.

38. Ilyas, R.N., et al. “Isolation and characterization of nanocrystalline cellulose from sugar palm fibres (Arenga Pinnata).” Carbohydrate Polymers 181 (2018):1038−1051.

39. Khawas, P., and Deka, S.C. “Isolation and characterization of cellulose nanofibers from culinary banana peel using high-intensity ultrasonication combined with chemical treatment.” Carbohydrate Polymers 137 (2016): 608−616.

40. Chen, W., et al. “Individualization of cellulose nanofibers from wood using high-intensity ultrasonication combined with chemical pretreatments.” Carbohydrate Polymers 83 (2011): 1804−1811.

41. Lu, P., and Hsieh, Y. “Preparation and properties of cellulose nanocrystals: Rods, spheres, and network.” Carbohydrate Polymers 82 (2010): 329−336.

42. Nagarajan, K.J., et al. “Extraction of cellulose nanofibers from cocos nucifera var aurantiaca peduncle by ball milling combined with chemical treatment.” Carbohydrate Polymers 212 (2019): 312–322.

43. Espino-Pérez, E., et al. “Green process for chemical functionalization of nanocellulose with carboxylic acids.” Biomacromolecules 15 (2014): 4551−4560.

44. Burhenne, L., et al. “The effect of the biomass components lignin, cellulose and

hemicellulose on TGA and fixed bed pyrolysis." Journal of Analytical and Applied Pyrolysis 101 (2013): 177−184

45. Xie, J., et al. "Isolation and characterization of cellulose nanofibers from bamboo using microwave liquefaction combined with chemical treatment and ultrasonication." Carbohydrate Polymers 151 (2016): 725–734.

46. Frone, A.N., et al. "Isolation of cellulose nanocrystals from plum seed shells, structural and morphological characterization." Materials Letters 194 (2017): 160−163.\

47. Wang, Z., et al. "Isolation and characterization of cellulose nanocrystals from pueraria root residue." International Journal of Biological Macromolecules 129 (2019): 1081–1089.

48. Zheng, D., et al. "Isolation and characterization of nanocellulose with a novel shape from walnut (Juglans Regia L.) shell agricultural waste." Polymers 11 (2019): 1130–1144.